

Spectroscopic Evaluation of the Nucleation and Growth for Microwave-Assisted CdSe/CdS/ZnS Quantum Dot Synthesis

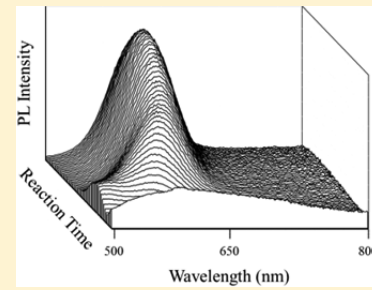
Andrew Zane,[†] Christie McCracken,[‡] Deborah A. Knight,[‡] W. James Waldman,[‡] and Prabir K. Dutta*,[†]

[†]Department of Chemistry and Biochemistry, The Ohio State University, Columbus, Ohio 43210, United States

[‡]Department of Pathology, The Ohio State University College of Medicine, Columbus, Ohio 43210, United States

Supporting Information

ABSTRACT: Use of microwave radiation to speed up the synthesis of CdSe-based quantum dots (QDs) in aqueous media is of practical interest and is the focus of this study. However, such microwave methods usually lead to low quantum yield (QY) QDs as compared to the conventional organic-based synthesis. By coupling the microwave oven with a fluorometer via a fiber optic cable, the fluorescence spectra during the QD evolution were obtained. Using the composition Cd₄:Se₁:Zn₄:MPA₂₀ (MPA = 3-mercaptopropionic acid), several stages of QD growth including development of CdSe nuclei, followed sequentially by CdS and then ZnS deposition were noted. The temperature of the microwave reaction between 130 and 155 °C led to QDs with similar QYs (17–19%), with the lower temperature taking longer to reach the optimal yield. The nucleation step was carried out at temperatures varying from 0 to 100 °C followed by growth in the microwave oven. With increasing temperature of nucleation, there was a red-shift in emission maximum, varying from 549 to 574 nm, with comparable QY, thus providing a route for QD size control in the microwave process. There was a profound effect of light illumination on the nucleated state prior to microwave treatment. Using light illumination, QDs with a QY of 40–41% were reproducibly obtained. With such optimized QDs, both flow cytometry and confocal microscopy of QD uptake into intestinal epithelial cells at 0.8–8 nM concentration were readily observed.



1. INTRODUCTION

Quantum dots (QDs) are nanosize semiconductors that fluoresce, the origin of fluorescence arising from quantum confinement effects. In a quantum dot, the particle size is smaller than the Bohr exciton radius, and this process manifests itself as an increase in the band gap energy.¹ Using this strategy with various semiconducting materials, nanometer-sized quantum dots have been made which fluoresce across the entire visible spectrum^{2–4} and in the infrared.⁵

QDs are useful in a variety of fields because they are less prone to photobleaching and chemical degradation, have discrete emission wavelengths based on size, and their wide absorption profile makes them very suitable for biological imaging.⁶ Materials scientists are exploring QDs for solar cells, sensors, and improved lighting.^{7–9}

Control of nucleation and growth of QDs is essential to optimize size and optical properties. Conventional organic-based hot-injection synthesis involves rapid nucleation by introducing precursor solutions to a hot (>300 °C) solvent. For the cadmium chalcogenides, these typically involve injection of dimethyl cadmium or cadmium oxide with other organometallic reagents into high temperature coordinating solvents such as trioctylphosphine (TOP) and trioctylphosphine oxide (TOPO).¹⁰ Controlled growth then occurs more slowly at a lower temperature, and the final size of the particles is determined by the temperature during the growth phase and the organic capping agent which sterically inhibits growth.¹⁰ Such methods of quantum dot production are well developed

and produce high quality quantum dots with quantum yields (QYs) between 50 and 80%.¹¹ The QY typically decreases with surface defects that create trap states, resulting in nonradiative decay and a broad red-shifted trap state emission.¹² To enhance the fluorescence and stability of the core particle, protective shells with a higher band gap are often grown around them.^{11,12}

Organically prepared quantum dots do not disperse in water and require ligand exchange, which can significantly alter the optical properties of the particles.¹³ Aqueous based methods of quantum dot synthesis have been developed which yield water-soluble quantum dots suitable for use in biological research. In these methods, cadmium chalcogenides (Se, Te) are nucleated by reacting cadmium salts (CdCl₂) with NaH(Se, Te) in the presence of a passivating ligand.^{14,15} These reaction methods have the benefit of being safer, less expensive, and yielding water-soluble particles without the need for ligand exchange; however, their quantum yield is typically lower compared to organic methods.

Microwave irradiation has been explored to decrease the time of aqueous quantum dot synthesis, and synthesis of CdSe(S), ZnSe(S), and CdSe/CdS/ZnS has been reported.^{16–19} Microwave heating of the precursors that are typically used in conventional convective heating has also been reported to produce QDs at shorter reaction times.^{20,21}

Received: May 14, 2014

Published: June 24, 2014



We have previously reported a fast, “one-pot” synthesis that produces stable, aqueous CdSe/CdS/ZnS core/shell quantum dots.¹⁸ While they are relatively easy to produce and show promising stability during biological experiments, these particles have a low quantum yield of 13%. In this research, we examine strategies for improving the quality of the microwave-produced QDs. By coupling the microwave reactor to a fluorescence spectrometer via fiber optics, the growth of the QD is monitored during synthesis, and this real-time data has provided insight into the growth mechanism. We also examine the effect of temperature during both the initial nucleation phase and the microwave-assisted crystal growth, and have found a way to form QDs with varying emission wavelengths. When combined with UV-visible light exposure during nucleation and after microwave-based QD growth, CdSe/CdS/ZnSe QDs with quantum yields of 40% were obtained.

2. EXPERIMENTAL SECTION

2.1. Typical Microwave Synthesis. Materials. Cadmium chloride hemipentahydrate ($\text{CdCl}_2 \cdot 2.5 \text{ H}_2\text{O}$, >98%) and sodium borohydride (NaBH_4 , 99%) were obtained from Aldrich (Milwaukee, WI, USA). Zinc chloride (ZnCl_2 , 99.99%), 3-mercaptopropionic acid (MPA), and selenium powder (Se, 99.5+, 200 mesh) were obtained from Acros (Geel, Belgium). Sodium hydroxide (NaOH) and ammonium hydroxide (NH_4OH , 28–30%) were obtained from Mallinckrodt Chemicals (Phillipsburg, NJ, USA). All chemicals were used without further purification. The H_2O used in this study was purified by a Barnstead NANOpure Infinity ultrapure water system (Dubuque, IA, USA).

Precursor Solutions. Cadmium/MPA. A 250 mL solution of 1.05 mM Cd and 5.26 mM MPA was prepared by adding 60 mg of cadmium chloride hemipentahydrate and 114.5 μL of MPA to approximately 225 mL of water. The pH was adjusted to 9.5 with 1 M NaOH, and the volume was adjusted to 250 mL in a volumetric flask. The final solution was stored in a plastic bottle and wrapped in aluminum foil.

Zn(NH_3)₄²⁺. A 25 mL solution of 26.67 mM Zn(NH_3)₄²⁺ was prepared using anhydrous zinc chloride and ammonium hydroxide. The hygroscopic zinc chloride was dried in a vacuum oven for 1 h at 200 °C and capped prior to weighing. To minimize error in weighing due to absorption of water from the air, approximately 90.9 mg of zinc chloride was quickly added to a previously weighed beaker containing 20 mL of water. Ammonium hydroxide was then added dropwise. A white precipitate formed and then disappeared as more ammonium hydroxide was added. Once the solution was fully clear, the volume of the solution was adjusted to 25 mL in a volumetric flask. The final solution was stored in a plastic bottle, wrapped in aluminum foil to protect from light, and stored at 4 °C.

NaHSe. A 152 mg portion of sodium borohydride was added to a glass test tube and chilled to 0 °C in an ethylene glycol/water bath. In quick succession, 2 mL of chilled water was pipetted into the test tube, followed by 158 mg of selenium powder. The test tube was capped with a rubber stopper with two needles sticking through, one of the needles attached to a nitrogen gas tank and the other left open to vent. The test tube was quickly placed back into the cold bath. The reaction showed intense bubbling from the evolution of hydrogen gas, which lasted for approximately 30 min. By this time, the black

selenium was reduced into the solution and a white $\text{Na}_2\text{B}_4\text{O}_7$ precipitate formed.

After completion, the vial was moved to a nitrogen filled glovebag. A 0.5 mL portion of the supernatant was pipetted into a 50 mL three-neck round-bottom flask containing 24.5 mL of nitrogen saturated water. This yielded a 25 mL solution of 20 mM NaHSe. The flask was kept capped, and nitrogen was constantly bubbled through the solution. Within 12–18 h, the presence of a red tint indicated that the selenium had oxidized, and the solution was no longer useful.

CdSe Nucleation. A 19 mL portion of the Cd/MPA solution was added to a 25 mL Erlenmeyer flask and vigorously stirred on a stir plate. A 0.25 mL portion of the NaHSe solution was quickly added, immediately resulting in a yellow color due to formation of CdSe nuclei. The solution was stirred for 1 h. After nucleation, 0.75 mL of the $\text{Zn}(\text{NH}_3)_4^{2+}$ solution was added. The final 20 mL solution was 1 mM Cd, 1 mM Zn, 0.25 mM Se, and 5 mM MPA. To nucleate the CdSe cores at various temperatures, the 19 mL Cd/MPA solution was added to a 25 mL round-bottom flask and heated in an oil bath under reflux. After the appropriate temperature was reached, the reflux was temporarily removed while the NaHSe solution was added via pipet under rapid stirring (1200 rpm). The solution was stirred for 1 h at the set temperature and allowed to cool to room temperature before addition of $\text{Zn}(\text{NH}_3)_4^{2+}$ and microwaving. Additionally, for lower temperatures, cores were nucleated at 0 °C by submerging the reaction flask into an ice bath.

Microwave-Assisted Growth. The solution was placed in a Discover SP (CEM Corp.) microwave system and heated for various times and temperatures, with the maximum power set to 200 W. After completion, the solution was cooled to 40 °C in the microwave with a stream of room temperature air, and then stored in a glass vial wrapped in aluminum foil at 4 °C until needed.

UV-Visible Light Aging. Samples were subjected to IR-filtered irradiation using a 150 W Xe lamp (model UXL151HXE, PTI) at room temperature under rapid stirring (1200 rpm). Samples were exposed to light for 2 h after initial 1 h nucleation, for 6 h after microwave crystal/shell formation, or both.

2.2. Particle Characterization. Optical Properties. UV-visible and fluorescence spectra were measured for QDs diluted 10:1 with water. Spectra were recorded with a Shimadzu UV-2501PC spectrophotometer. Fluorescence measurements were recorded with a Horiba Jobin-Yvon Fluorolog 3, using 2 nm slit widths for the emission and excitation monochromators, 0.3 s integration time, and a 375 nm excitation wavelength. The instrument was equipped with a photomultiplier tube detector.

Quantum yields were measured using a Quanta-Phi integrating sphere attachment for the Fluorolog 3. The detector was set to measure counts rather than the default counts per second. Slit widths for the emission and excitation monochromators were set to 5 nm, and the samples were excited with 480 nm light. Spectra were measured from 460 to 750 nm, to include both the excitation and emission wavelengths. An initial blank water sample was measured, adjusting the integration time to obtain an excitation peak height of 1 million counts to avoid oversaturation of the detector. The sample was then measured using the same settings for comparison. The areas under the excitation and emission curves in each spectrum were integrated, allowing for calculation of the quantum yield:

$$QY = \frac{\text{emission}_{\text{sample}} - \text{emission}_{\text{blank}}}{\text{excitation}_{\text{blank}} - \text{excitation}_{\text{sample}}} \times 100\%$$

Fluorescence lifetime was measured with the Fluorolog 3 time correlated single photon counting (TCSPC). Fluorescence was excited with a pulsed 455 nm LED (1.5 ns pulse duration). The repetition rate was set to 1 MHz.

In Situ Fluorescence. *In situ* fluorescence measurements were taken during the microwave irradiation step of the synthesis. The Discover SP system is configured with a porthole for use with a camera attachment. We were able to couple the fluorometer to the microwave reactor via the camera porthole using a fiber optic cable attachment. Figure 1 shows a close-up of the fiber-optic inserted into the camera port inside of the microwave.

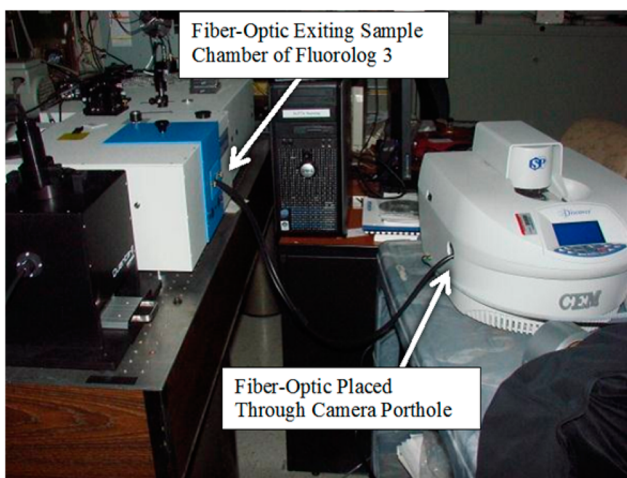


Figure 1. Fiber optic coupling of the fluorometer (Fluorolog 3) with the microwave oven (Discover SP) allowing for *in situ* fluorescence measurements during synthesis.

Batch runs were set up using the fluorometer software to take approximately one spectrum every minute. A significant fluorescence near 500 nm was present when the typical 375 nm excitation wavelength was used. This peak was observed when no sample was present, and is attributed to the lining of the microwave chamber. An excitation wavelength of 480 nm was chosen, which adequately stimulated quantum dot emission while avoiding the background fluorescence of the microwave chamber. A 6 nm bandwidth was used for both the excitation and emission monochromators. The emission wavelength was scanned from 500 to 750 nm with an integration time of 0.2 s.

X-ray Diffraction. As-prepared QD solutions were washed twice with water by centrifugation (290 000g), replacement of supernatant, and redispersion. After the second wash, particles were dried overnight in a vacuum oven. The sample was loaded into a 0.5 mm capillary, and XRD spectra were recorded using a Bruker D8-advance system with nickel-filtered Cu K α radiation (1.5405 Å).

Electron Microscopy. High resolution transmission electron microscopy (HRTEM) images were obtained using a Tecnai-F20 system. Particles were washed twice by centrifugation and replacement of supernatant, resuspended in a dilute solution in ethanol, and deposited onto a lacey-carbon coated copper grid.

Biological Imaging. Cell Culture. C2BBe1 cells were obtained from the American Type Culture Collection (Manassas, VA). Cells were cultured in Dulbecco's Modified

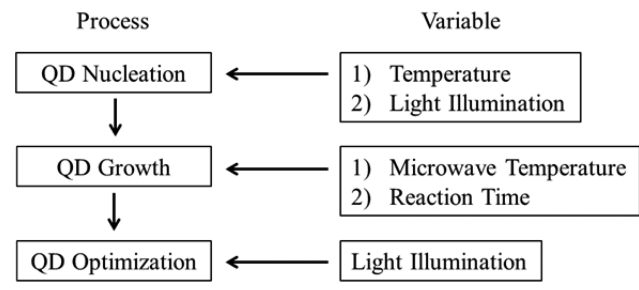
Eagle Medium (DMEM; Life Technologies, Grand Island, NY) supplemented with 10% fetal bovine serum (FBS; Serum Source International, Inc., Charlotte, NC), 1 mM sodium pyruvate, 2 mM L-glutamine, 0.3% penicillin/streptomycin, 0.3 μ g/mL Amphotericin B (fungizone), and 10 μ g/mL transferrin (all from Life Technologies). Cells were incubated in 5% CO₂/95% room air at 37 °C. Cells were passaged every 5–7 days and plated on flasks or plates precoated with collagen I (0.05 mg/mL, rat tail, Life Technologies). Cells were plated at a density of 70 000 cells/well in 24-well tissue culture plates (Corning-Costar, Tewksbury, MA) for comparison of QD fluorescence intensity by flow cytometry. Cells were plated in 8-chamber slides (Thermo Scientific) at a density of 90 000–100 000 cells/chamber for analysis by confocal microscopy. Cells were incubated for at least 24 h after plating before treatment with QDs. Directly prior to treatment on cells, QDs were sonicated using a Sonics Vibra-Cell sonicator (Sonic Materials, Inc., Norwalk, CT) pulsing for 1 s on, 1 s off for approximately 15 s in order to minimize QD agglomeration. Experiments were generally performed at a dose of 157 nM which was achieved by adding 107 μ L of the QDs (732 nM) per well in a 24-well plate with a 0.5 mL total volume per well with cell culture media and 64 μ L of QDs per chamber in an 8-chamber slide with a total volume of 0.3 mL per chamber. After treating cells with the appropriate dose of QDs, cells were centrifuged to promote contact of QDs with cells. The 24-well plates were centrifuged at 300g for 15 min. Due to greater fragility, 8-chamber slides were centrifuged at 75g for 15 min. Cells were incubated with QDs for 24 h before performing experiments.

Flow Cytometry. After 24 h treatment of cells with QDs, cells were washed twice with phosphate-buffered saline (PBS) and detached from the culture plate with trypsin. Cells were suspended in PBS and analyzed for fluorescence using a FACScalibur flow cytometer (BD Biosciences, San Jose, CA) at an excitation wavelength of 488 nm. All experimental treatments were performed in triplicate. Mean fluorescence intensity values were used to compare the fluorescence of QDs made by different syntheses in cells.

Confocal Microscopy. After 24 h treatment of cells with QDs, the chambers were removed from 8-chamber slides for staining. All staining was performed at room temperature. Slides were washed twice with PBS and fixed in 4% paraformaldehyde for 45 min. Cells were washed again in PBS before permeabilization in a 0.2% Triton X-100 (Sigma-Aldrich) solution in PBS for 15 min. Cells were washed in PBS and incubated in a 1% bovine serum albumin (BSA; Sigma-Aldrich) blocking solution for 1 h. Cells were incubated with a 1:150 dilution of Alexa Fluor 647 mouse anti-E-cadherin (BD Biosciences) in 1% BSA in PBS for 90 min. Cells were washed with PBS and stained with a 0.25 μ g/mL solution of 4',6'-diamidino-2-phenylindole (DAPI, Life Technologies) in 1% BSA in PBS for 10 min. Cells were washed with PBS before coverslips were mounted using ProLong Gold Antifade Reagent (Life Technologies). Mounting media was allowed to cure overnight at room temperature before analysis using a Zeiss LSM 700 confocal fluorescence microscope (Jena, Germany).

3. RESULTS

3.1. Synthetic Strategies. Scheme 1 shows the synthetic pathways discussed in this paper. The overall composition Cd₄:Se₁:Zn₄:MPA₂₀ is maintained the same for all experiments. The effect of temperature during the microwave heating phase of the synthesis was examined between 125 and 160 °C in S°

Scheme 1. QD Synthesis and Optimization Strategy

increments. At temperatures below 125 °C and above 160 °C, very weakly fluorescent products were obtained. Only the reactions between 130 and 155 °C were studied further. The fluorescence of the quantum dots was observed *in situ*. To determine an approximate reaction time for each temperature, the time at which the fluorescence of the quantum dot stopped increasing was chosen on the basis of the *in situ* data. Approximate reaction times varied from 27 min at 155 °C to 4 h and 20 min at 130 °C for a room temperature nucleated sample. Using these reaction times as a starting point, the optimal time for each temperature was determined by performing the synthesis at several times bracketing this time, and measuring the quantum yields of all recovered samples. This process was repeated with nucleation of CdSe between 0 and 100 °C, followed by microwave irradiation (MWI) at temperatures between 130 and 155 °C for time periods ranging from 45 to 340 min. In addition, UV-visible light illumination was carried out during nucleation as well as after microwave treatment.

3.2. Room Temperature Nucleation. The nucleation of CdSe during the initial mixing of Cd²⁺, NaHSe, and 3-MPA was examined over a range of temperatures. We focus first on the room temperature nucleated samples. To examine the initial steps during this nucleation event, the sulfur source 3-MPA was omitted from the reaction. Without 3-MPA, there was immediate formation of bulk CdSe particles upon mixing the cadmium and NaHSe solutions, indicating that the role of 3-MPA is crucial in complexing the Cd²⁺, and gradually releasing it to react with the NaHSe. The second set of experiments excluded the Zn(NH₃)₄²⁺ and was heated in the microwave at 150 °C. The reactions were stopped at 10 min intervals, the solution was cooled, and the fluorescence spectrum was measured. Figure 2 shows that there is an initial broad emission peak at 502 nm, along with a trapped state band at 705 nm. Both of these bands disappear, along with growth of a band at 537 nm, which red-shifts to 545 nm in 30 min and increases in intensity. With further heating, the 545 nm emission decreases in intensity and red-shifts to 557 nm. At the conclusion of the experiment at 100 min, the solution had a dark red color and broad, strong emission at >700 nm from trap states.

A similar experiment was repeated with all of the reactants, but here the fluorescence spectra were recorded by removing the solution at 10 min intervals, and diluting it by a factor of 10 before recording the spectra. As Figure 3 shows, there is a broad band at 517 nm at 10 min, which gradually red-shifts and increases in intensity, reaching a maximum at 559 nm at 80 min. The trapped state emission is significantly quenched in the presence of zinc.

In order to evaluate the intermediate steps during the microwave treatment without disturbing the system, *in situ* fluorescence measurements were carried out. Figure 4a shows a

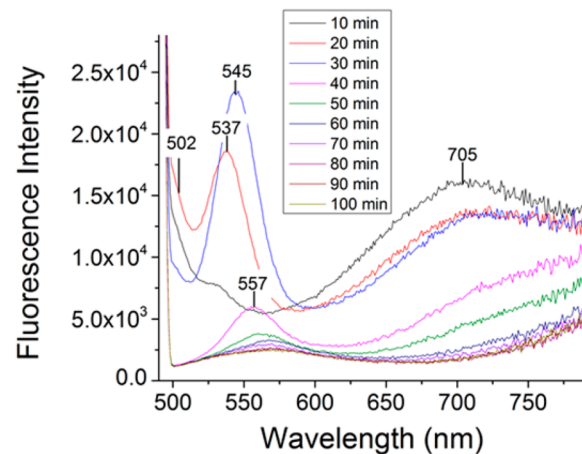


Figure 2. Fluorescence spectra of the composition Cd₄:Se₁:MPA₂₀ heated in the microwave at 150 °C, with spectra recorded at room temperature while in the microwave after heat treatment every 10 min, $\lambda_{\text{ex}} = 480$ nm.

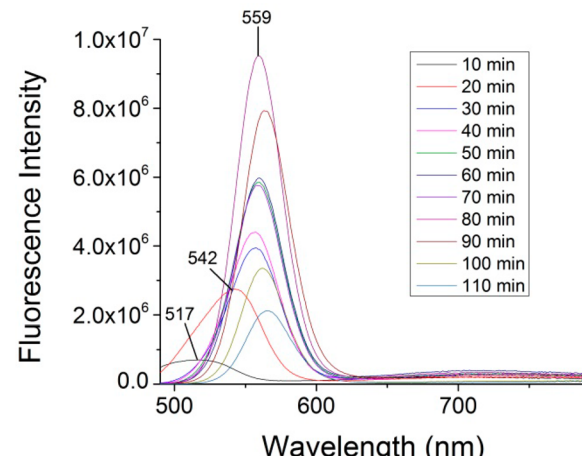


Figure 3. Fluorescence spectra for the composition Cd₄:Se₁:Zn₄:MPA₂₀ at 150 °C, stopped at 10 min intervals, removed from the microwave, cooled to room temperature, diluted by a factor of 10, and spectrum recorded, $\lambda_{\text{ex}} = 375$ nm.

three-dimensional plot of the *in situ* time-dependent fluorescence at the temperature of microwave operation, 150 °C (*x* and *y* axes are the emission wavelength and time, respectively, and the *z* axis is the intensity). Within 20 min, a band at 502 nm is observed. This band disappears over the next 20 min, as the band around 550 nm develops, which gradually red-shifts to 574 nm and grows in intensity. After 60 min, the band at 574 nm decreases. This can be compared with Figure 3, where an identical reaction was carried out but was cooled to room temperature and diluted before the spectra were recorded. When the spectra are recorded at room temperature instead of *in situ* at 150 °C, the optimal fluorescence intensity is observed at 80 rather than 60 min, and λ_{max} at 556 rather than 574 nm. This is because, at higher temperatures, λ_{max} red-shifts and the intensity decreases, due to change in the relative position of the conduction and valence bands from a temperature-dependent change in lattice dilatation and electron lattice interactions.²²

Figure 4b shows another view of the data in Figure 4a, starting from the lowest fluorescence intensity 5 min into the experiment and ending with the maximum fluorescence

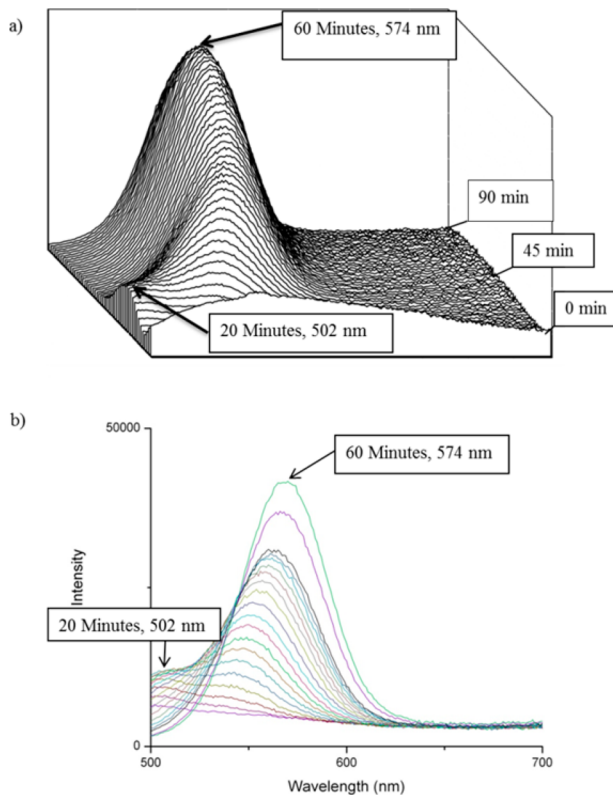


Figure 4. *In situ* fluorescence spectrum recorded during microwave heating at 150 °C. (a) Overview shows development of early emission at 502 nm, giving way to main QD emission. (b) Superposition of the spectra recorded during the first 60 min of part a. $\lambda_{\text{ex}} = 480$ nm.

intensity 60 min into the experiment. Simultaneous growth of two emissions, one at 502 nm and one starting near 540 nm, occurs in the first 20 min of the synthesis. The 502 nm emission begins to decrease in intensity, and the 540 nm emission gradually red-shifts to 574 nm, and increases gradually in intensity. An isosbestic point at 550 nm is observed between times of 40 and 60 min, indicating that, within this time period, two species are interconverting.

The microwave synthesis was repeated as a function of temperature. Using the *in situ* fluorescence to monitor the times around which the fluorescence reached its maximum, the appropriate time for each temperature was optimized for the range of 130–155 °C. At temperatures higher or lower than this range, the fluorescence spectra were significantly degraded, and not discussed in this study. Figure S1 (Supporting Information) shows all of the *in situ* data as a function of time for each temperature. Table 1 shows the samples at each temperature with the optimal quantum yield. Similar quantum

yields (QY, 17–19%) were obtained at all microwaving temperatures between 130 and 155 °C, as long as the time for microwave treatment is optimized. Lower temperatures required longer times to reach the optimum QY.

Figure 5a,b shows a plot of the peak fluorescence intensity with time at 135 and 155 °C. There is an increase in intensity

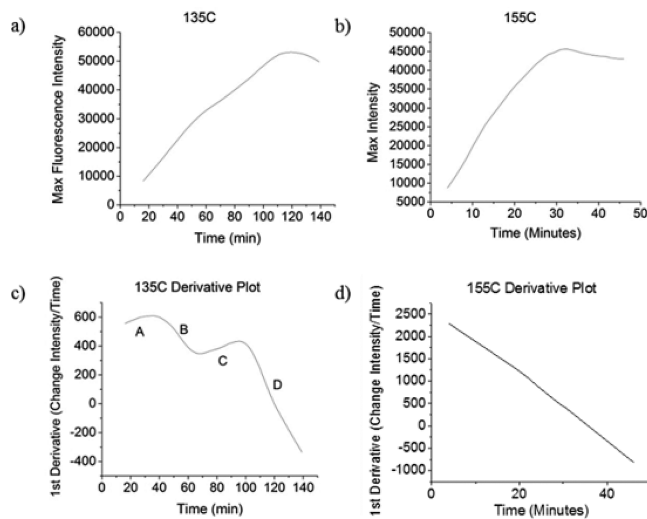


Figure 5. Plot of the maximum intensity of the *in situ* fluorescence as a function of time for synthesis at (a) 135 °C and (b) 155 °C and the corresponding derivative plots as a function of time for (c) 135 °C and (d) 155 °C.

before leveling off or decreasing during the final 10–15% of the monitored time. The derivative plots (rate of change in intensity with time, Figure 5c,d) provide further insight. In particular, the data at 135 °C shows four distinct regions. Region A between 10 and 30 min depicts an upward slope, region B has a downward slope (though still positive growth in fluorescence intensity), while region C again has an upward slope between 70 and 100 min. Region D beyond 120 min exhibits a decreasing rate of fluorescence intensity. As the temperature was raised to 155 °C, all stages merged into one another with a downward slope (all positive until the final 10% of the reaction).

3.3. Nucleation at Various Temperatures. The nucleation step was carried out between 0 and 100 °C, followed by microwave treatment at 150 °C for 80 min, and the fluorescence spectra and QY were measured. Figure 6 shows that the emission maximum is altered systematically with nucleation at different temperatures, with the 0 °C emitting at 546 nm and that at 100 °C at 574 nm. Table 2 shows the characteristic λ_{max} (nm) and QY of the samples obtained as a function of the various nucleation temperatures. Except for the sample nucleated at 0 °C, all other samples exhibited a QY of 17–18%.

The *in situ* fluorescence experiments over the range of temperatures 130–155 °C were repeated with the sample nucleated at 100 °C, and these data are shown in Figure S2 (Supporting Information). The data appear similar to the spectra recorded with the room temperature nucleation. Figure S3 (Supporting Information) shows the derivative plots for the 100 °C nucleated sample; four different slopes for the reaction at 130 °C are observed.

3.4. Effects of Light Illumination. The influence of UV-visible irradiation during nucleation was examined with two

Table 1. Quantum Yields for a Room Temperature Nucleated Sample Heated in the Microwave at 130–155 °C for Optimal Times for Best QY

reaction temperature (°C)	optimal time (min)	quantum yield (%)
130	340	17
135	170	18
140	110	19
145	95	18
150	75	19
155	45	19

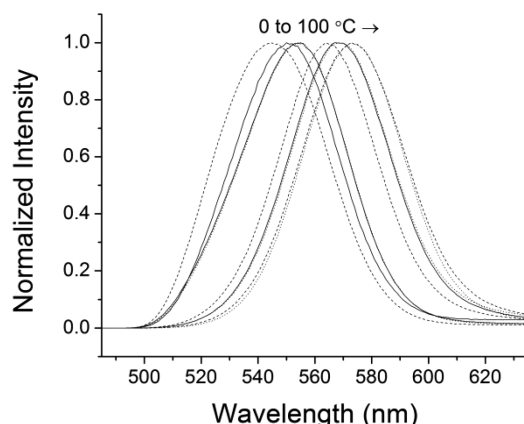


Figure 6. QDs nucleated from 0 to 100 °C and reacted in a microwave at 150 °C for 80 min, showing a red-shift of the λ_{max} with increasing nucleation temperature, $\lambda_{\text{ex}} = 375$ nm.

Table 2. λ_{max} and Quantum Yield Values of QDs Nucleated from 0 to 100 °C and Then Reacted in the Microwave at 150 °C for 80 min

nucleation temperature (°C)	λ_{max} (nm)	quantum yield (%)
0	546	8
22	551	17
40	555	18
50	556	18
60	565	17
70	569	17
80	568	17
90	574	17
100	574	18

samples, one nucleated at room temperature and the second nucleated at 100 °C. Samples that were irradiated for 2 h were then heated in the microwave at 150 °C for 80 min. Table 3

Table 3. Summary of Light Illumination Experiments Both Pre-Microwave (during Nucleation) and Post-Microwave (after Synthesis)

nucleation temperature	light treatment	λ_{max}	quantum yield
22 °C	none	549 nm	19%
	2 h pre	537 nm	3%
	6 h post	548 nm	28%
	2 h pre/6 h post	539 nm	15%
100 °C	none	574 nm	18%
	2 h pre	574 nm	19%
	6 h post	574 nm	31%
	2 h pre/6 h post	574 nm	40%

lists the QY of the various samples. These data show that light illumination during room temperature nucleation decreases the QY considerably (19 to 3%), while for the 100 °C nucleated sample, the QY remained unchanged (18 to 19%). Illumination after the microwave treatment was also carried out for a period of 6 h. Table 3 shows that, for the room temperature nucleation, the QY almost recovered (15%), but for the sample nucleated at 100 °C, the QY reached 40%. Illumination only after the microwave treatment did improve the QY for both room temperature and 100 °C nucleated samples from 19 to 28% and 18 to 31%, respectively. Thus, light illumination

during the nucleation period is having a negative effect on the room temperature nucleated sample but a positive effect on the sample nucleated at 100 °C. With UV-visible light illumination both during the nucleation and after microwave treatment, there were marked improvements in the QY. For the room temperature nucleation, the QY increased from 3 to 15%, and for the sample nucleated at 100 °C, the QY increased from 19 to 40%. Several syntheses were repeated with the sample nucleated at 100 °C, with the QY always between 40 and 41%.

3.5. Characterization of Final QDs. We characterized the QD sample with the 40% QY, and Figure 7 shows the optical spectra, TCSPC, XRD, and TEM of this sample. The absorption maximum is observed at 542 nm, with peak emission at 574 nm (Figure 7a). Figure 7b shows the high resolution TEM; 20 particles were selected in the TEM, and an average diameter of 4.6 ± 0.3 nm was calculated for the QD. The image in the inset shows lattice fringes with a spacing of 0.33 nm, which extend out to the edges of the crystal indicative of a single crystal. Figure 7c shows the lifetime (TCSPC) data, and was best fit by a three-exponential equation (lifetimes, 3.3, 16, 110 ns), with a majority contribution from the 16 ns lifetime which falls in a range typically reported for QDs in the literature.^{19,23,24} The 3.3 ns contribution is possibly arising from QDs with surface traps.¹⁹ We assign the longer lifetime component at 110 ns to an impurity, since its contribution decreases as we dialyze the QD samples. We could not get rid of it completely, since, with dialysis, the MPA capping ligand is also lost and the QDs become unstable. Figure 7d shows the XRD pattern with four broad peaks at 26.6, 43.9, 45.8, and 52.2° (2θ). The figure also shows the expected patterns of the wurtzite and zinc blende structure of CdSe, CdS, and ZnS. Because of the width of the bands, it is difficult to pinpoint the structure, but because the peak at 45.8° appears to match closely the (1 0 3) plane of the wurtzite structure of CdSe, we assign the QD to have a wurtzite structure with all three chalcogenides of this form.^{2,25}

3.6. Biological Imaging Studies. We have reported previously imaging of microwave-based QDs with QY < 20% in macrophages.¹⁸ With the present QDs with twice the QY, we examined the improvement possible for biological imaging. These experiments were performed in C2BBe1 cells,²⁶ which are a human intestinal epithelial cell line, and relevant for uptake of food-relevant nanoparticles.²⁷ Comparing mean fluorescence intensities (MFIs) in a flow cytometry experiment revealed that fluorescence could be reliably detected only in cells treated with the QDs (40% QY) at concentrations of 8–39 nM (Figure 8a), as compared to the QDs with 19% QY. The flow cytometer will detect fluorescence in cells that have both internalized and membrane-bound QDs. Thus, to investigate internalization, fluorescence confocal microscopy was carried out and QDs with 40% QY were detected at concentrations as low as 0.8 nM.

4. DISCUSSION

The advantages of microwave heating for synthesis of QD have been enumerated.^{3,17,20} Besides uniform dielectric heating of the reaction volume, influence on the collisions between reactants as well as entropic effects due to the rotation of the dipoles are considered important in explaining kinetics and reaction yields. We have reported earlier that, with the composition $\text{Cd}_4\text{Se}_1\text{Zn}_4\text{MPA}_{20}$, microwave synthesis led to a QD of nominal structure with a CdSe core and an alloyed shell involving CdS and ZnS, and represented the QD as CdSe/

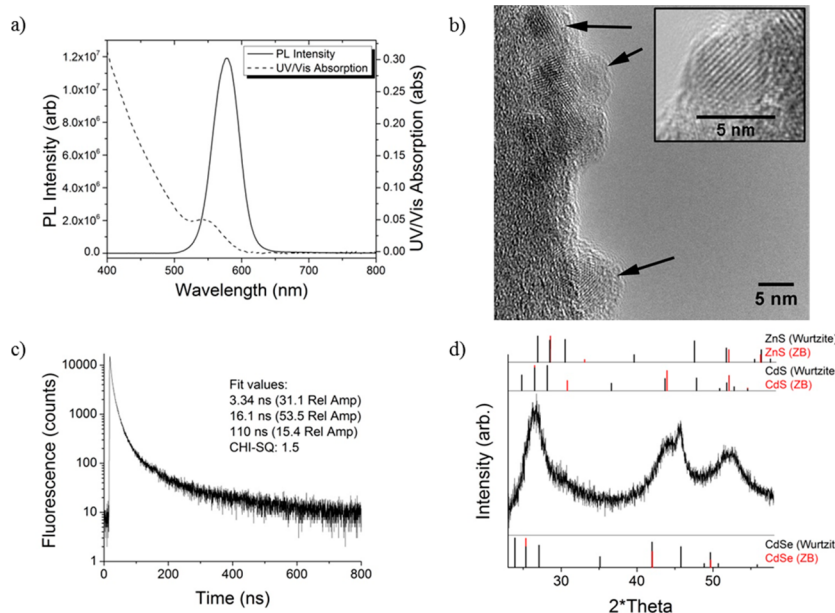


Figure 7. Characteristics of the QD with 40% QY. (a) UV-vis absorption and fluorescence spectra. Absorption maximum at 542 nm, emission maximum at 574 nm. (b) Representative HRTEM image, average diameter 4.6 ± 0.3 nm calculated from 20 particles. The inset shows a close-up of a 4.3 nm particle with clearly visible lattice fringes, measured to be 0.33 ± 0.02 nm. (c) Fluorescence lifetime (TCSPC) decay curve, 455 nm LED light source with a pulse width of 1.3 ns. Data was best fit to a three-exponential curve with lifetimes of 3.3, 16.8, and 110 ns. (d) Baseline corrected capillary XRD pattern. Peak positions are 26.6, 43.9, 45.8, and 52.2° (expected peaks for wurtzite and zinc blende (ZB) structures of the three chalcogenides are also shown).

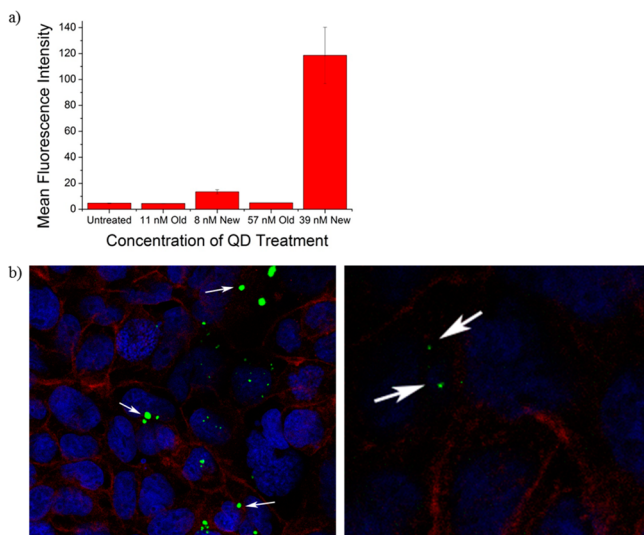


Figure 8. Biological imaging. (a) Flow cytometry showing the mean fluorescence intensity of cells treated for 24 h with QDs nucleated at room temperature (19% QY, old) and optimized QDs nucleated at 100 °C (40% QY, new). (b) Confocal microscopy of cells treated with 16 nM (left) and 0.8 nM (right) QDs (40% QY) for 24 h.

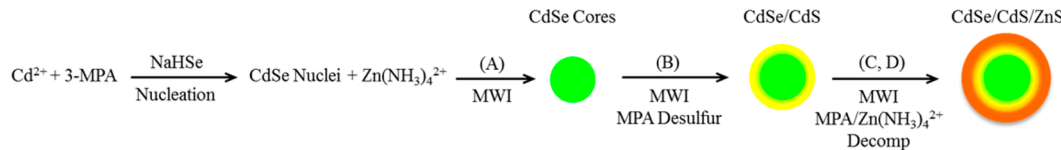
CdS/ZnS. The QYs of these QDs were <15%. In the present paper, we examine the same composition, with the goal to understand and optimize this synthesis, and evaluate the mechanistic steps involved in the synthesis. The use of fluorescence spectroscopy during the microwaving process is also being used for the first time; previous efforts have reported on the use of infrared spectroscopy.²⁸

4.1. QD Growth Mechanism. We propose a reaction mechanism for the microwave synthesis of the QDs. A population of CdSe seed nanoparticles forms immediately

upon mixing cadmium and selenium ions. These particles are protected from aggregation and further reactions by the thiol-linked protection of 3-MPA, since, as noted, the absence of 3-MPA leads to formation of bulk CdSe. With 3-MPA, but in the absence of $Zn(NH_3)_4^{2+}$, an emission band at 502 nm is formed immediately in the microwave at 150 °C, and persists for about 20 min and is replaced gradually with a band at 545 nm (Figure 2). The particles emitting at 545 nm are due to CdS deposition on the CdSe nuclei, the red-shift occurring from the higher band gap shell deposition. The CdS cap forms after 3-MPA decomposition and the resulting release of sulfur. The QD isolated from this reaction has poor optical properties, with large trap state emissions. QDs with a CdSe core and a predominantly CdS shell with a gradient alloy shell structure prepared in the microwave have been reported.¹⁶ Previous aqueous based thioalcohol-capped CdSe and CdTe QDs were found to have low QYs.^{14,22}

In the presence of $Zn(NH_3)_4^{2+}$, the growth process continues with the Zn^{2+} depositing as an outer shell ZnS on the CdSe/CdS particles. Figure 3 shows that deposition of ZnS results in a red-shift of the emission. The isosbestic point in Figure 4b is assigned to the disappearance of the CdSe/CdS particle (at 545 nm) and the formation of the CdSe/CdS/ZnS QD (emitting at 575 nm). This would indicate that the ZnS deposition occurs later than CdS because of the higher energy necessary to decompose the $Zn(NH_3)_4^{2+}$ complex.

The derivatives of the peak fluorescence intensity obtained during the *in situ* experiments provide more insight. The four regions in Figure 5c for the room temperature nucleated sample and heated in the microwave at 135 °C (Figure S3, Supporting Information, shows similar data for a sample nucleated at 100 °C) can be correlated with the observations above as follows. Region A between 10 and 30 min depicts an upward slope, and is related to the growth of the CdSe nuclei. Region B has a downward slope (though still positive growth in

Scheme 2. Synthetic Pathway of CdSe/CdS/ZnS Microwave Assisted Synthesis**Table 4. Comparison of QYs of Water-Soluble Microwave-Based CdSe/ZnS QDs Reported in the Literature**

reference	QY	comments
Roy et al. ²¹	28%	Organic-based core synth. in microwave, 150 °C for 2 min. Water-soluble shell addition.
Han et al. ¹⁹	38%	Citrate capped, core and shell separately synthesized, MWI 120 °C for 2 min each.
Schumacher et al. ¹⁸	13%	MPA capped, room temperature nucleated, MWI 150 °C 90 min.
Luan et al. ³⁷	28%	Organic-based synthesis, MPA ligand exchanged. No MWI, 285 and 260 °C nucleation and growth temperatures.
Zhang et al. ³⁸	26–33%	Organic-based synthesis, MPA ligand exchanged. QY increase to 33% after functionalization with denatured transferrin.
this paper	40%	MPA capped, 100 °C nucleation with UV-vis irradiation, MWI 150 °C 80 min, 6 h UV-vis irradiation post-treatment.

fluorescence intensity) and is proposed to arise from the deposition of the CdS shell. Region C is the incorporation of the ZnS shell. Region D continues with the incorporation of the ZnS shell, but as the quality of the QD improves, the self-quenching of the QDs becomes more pronounced, and leads to a decreasing rate of fluorescence intensity. If the microwaving temperature is increased to 155 °C, these regions merge into one another (Figure 5d). Similar observations were also made with the sample nucleated at 100 °C (Figures S2 and S3, Supporting Information).

The reaction temperature during the microwave process does not impact the optical properties of the QDs, as long as the temperatures are within the range 130–155 °C (Table 1), and enough time is given to reach the optimized state. The unchanged λ_{max} with microwave temperature (Table 1) indicates that the nuclei formed during the nucleation are responsible for the final optical properties of the QD. The microwave temperature is influencing the rates at which the various processes occur, including growth of nuclei by incorporation of the limiting nutrients, deposition of CdS, and then ZnS. With continued microwave treatment beyond the optimum time at a fixed temperature, the QY drops, and can be related to deposition of thicker ZnS layers.^{2,30} Also, at microwave temperatures exceeding 155 °C, the QY decreases, and could be due to deposition of thicker ZnS layers, and extensive MPA decomposition, with loss of the surface passivation of QD. Scheme 2 provides a mechanistic description of the growth.

4.2. Controlling λ_{max} of Emission. As observed in Figure 6, the primary effect of the temperature at which CdSe cores are formed prior to microwave irradiation is to alter the emission maximum, with the peak emission wavelength red-shifting from 549 to 574 nm. At the lower temperature of nucleation, smaller size nuclei are formed, since the Cd²⁺ is coordinated with the MPA. The influence of ligand detachment on growth of ZnSe QDs has been carefully studied.³¹ As nucleation temperatures increase, more of the Cd²⁺ is released, forming larger nuclei, assisted by ligand detachment from the surface of the nucleated state. Once these nuclei are subjected to microwave, they grow into CdSe cores, with the lower temperature nucleated state producing smaller CdSe cores and more of them as compared to the higher temperature nucleation, since the nutrient pool is the same in all cases. Thus, for a fixed composition, making fewer nuclei by

manipulating the nucleation temperature controls the core particle size.

4.3. Improving Quantum Yield. There have been many reports on improvement in QY by light illumination after QD synthesis.^{32–36} The improvement arises from dissolution of surface defects and their passivation. We show that light illumination during nucleation is also a method to manipulate nuclei structure. Indeed, as Table 3 shows, light illumination during nucleation (2 h) and after microwave treatment (6 h) had a profound effect on the QY, especially for the nucleation carried out at 100 °C. The QY is improved considerably (18% → 40%), with unchanged λ_{max} at 574 nm. For the nucleation at 22 °C, illumination during nucleation followed by microwaving led to a significant decrease in QY (19% → 3%), which could be improved by illumination after microwave treatment (QY: 19% → 28%). We explain these results as arising from the fact that the nuclei formed at 22 °C are less stable with irradiation. Nanocrystals of CdTe with a large defect structure have been reported to dissolve during photochemical etching.²⁹ However, for the nuclei prepared at 100 °C, the nuclei are larger and more stable. Light illumination restructures the surface, vacancies can be satisfied with the 3-MPA, and there will be minimal change in size. This restructured surface is further improved with post-microwave illumination. Table 4 summarizes the current literature on microwave synthesized aqueous CdSe/ZnS QDs. To date, the highest quality microwave synthesized aqueous CdSe/ZnS particles were 38% quantum yield, and thus the method reported in this paper is an improvement.

4.4. Biological Imaging. The biological imaging studies shown in Figure 8 clearly demonstrate that, with the higher QY (40%), both flow cytometry and confocal imaging can be done with more dilute concentrations of QDs. From a biological perspective, the uptake of QDs by the epithelial C2BBe1 cells is of interest, since nanoparticles used in food can enter the circulation and be further distributed once transported through these epithelial cells, and thus QDs can be used as a model for evaluating the rate of uptake of nanoparticles by these cells.

5. CONCLUSIONS

Several synthetic strategies for QD synthesis all starting with the composition Cd₄:Se₁:Zn₄: MPAs₂₀ are being reported. *In situ* fluorescence spectroscopy during microwave synthesis of the QD provided insight into the growth process, including growth of the CdSe nuclei and deposition of the CdS and ZnS shell

layers. The temperature during the microwave treatment (130–155 °C) led to QDs with the same QY and λ_{\max} . Changing the nucleation temperature (0–100 °C) prior to microwave growth produced QDs of varying size and with increasing λ_{\max} (range 546–574 nm). UV-visible light illumination in the nucleation step and post-microwave treatment led to optimal QDs with QYs of 40–41%. These QDs were examined as biological imaging agents. Uptake of QDs into intestinal epithelial cells could be readily observed at 0.8–8 nM QD concentrations by confocal microscopy and flow cytometry, respectively.

ASSOCIATED CONTENT

Supporting Information

In situ fluorescence data for all microwave temperatures 135–155 °C for both room temperature and 100 °C nucleated particles, along with maximum intensity plots for 100 °C nucleated samples. This material is available free of charge via the Internet at <http://pubs.acs.org>.

AUTHOR INFORMATION

Corresponding Author

*E-mail: dutta@chemistry.ohio-state.edu. Phone: (614) 292-4532.

Notes

The authors declare no competing financial interest.

ACKNOWLEDGMENTS

We acknowledge funding from USDA/NIFA (2011-67021-30360) for this research. We thank Hendrik Colijn for the TEM data.

ABBREVIATIONS

QD, quantum dot; QY, quantum yield; MPA, 3-mercaptopropionic acid; TCSPC, time-correlated single photon counting; PBS, phosphate buffered saline; MWI, microwave irradiation

REFERENCES

- (1) Brus, L. E. A Simple Model for the Ionization Potential, Electron Affinity, and Aqueous Redox Potentials of Small Semiconductor Crystallites. *J. Chem. Phys.* **1983**, *79*, 5566.
- (2) Dabbousi, B. O.; Rodriguez-Viejo, J.; Mikulec, F. V.; Heine, J. R.; Mattoussi, H.; Ober, R.; Jensen, K. F.; Bawendi, M. G. (CdSe)ZnS Core–Shell Quantum Dots: Synthesis and Characterization of a Size Series of Highly Luminescent Nanocrystallites. *J. Phys. Chem. B* **1997**, *101*, 9463–9475.
- (3) Li, L.; Qian, H.; Ren, J. Rapid Synthesis of Highly Luminescent CdTe Nanocrystals in the Aqueous Phase by Microwave Irradiation with Controllable Temperature. *Chem. Commun.* **2005**, 528–530.
- (4) Bowers, M. J.; McBride, J. R.; Rosenthal, S. J. White-Light Emission from Magic-Sized Cadmium Selenide Nanocrystals. *J. Am. Chem. Soc.* **2005**, *127*, 15378–15379.
- (5) Ma, Q.; Su, X. Near-Infrared Quantum Dots: Synthesis, Functionalization and Analytical Applications. *Analyst* **2010**, *135*, 1867–1877.
- (6) Resch-Genger, U.; Grabolle, M.; Cavaliere-Jaricot, S.; Nitschke, R.; Nann, T. Quantum Dots versus Organic Dyes as Fluorescent Labels. *Nat. Methods* **2008**, *5*, 763–775.
- (7) Hyldahl, M. G.; Bailey, S. T.; Wittmershaus, B. P. Photo-Stability and Performance of CdSe/ZnS Quantum Dots in Luminescent Solar Concentrators. *Sol. Energy* **2009**, *83*, 566–573.
- (8) Lee, K. S.; Lee, D. U.; Choo, D. C.; Kim, T. W.; Ryu, E. D.; Kim, S. W.; Lim, J. S. Organic Light-Emitting Devices Fabricated Utilizing Core/shell CdSe/ZnS Quantum Dots Embedded in a Polyvinylcarbazole. *J. Mater. Sci.* **2011**, *46*, 1239–1243.
- (9) Jang, E.; Jun, S.; Jang, H.; Lim, J.; Kim, B.; Kim, Y. White-Light-Emitting Diodes with Quantum Dot Color Converters for Display Backlights. *Adv. Mater.* **2010**, *22*, 3076–3080.
- (10) De Mello Donegá, C.; Liljeroth, P.; Vanmaekelbergh, D. Physicochemical Evaluation of the Hot-Injection Method, a Synthesis Route for Monodisperse Nanocrystals. *Small* **2005**, *1*, 1152–1162.
- (11) Hines, M. A.; Guyot-Sionnest, P. Synthesis and Characterization of Strongly Luminescing ZnS-Capped CdSe Nanocrystals. *J. Phys. Chem.* **1996**, *100*, 468–471.
- (12) Spanhel, L.; Haase, M.; Weller, H.; Henglein, A. Photochemistry of Colloidal Semiconductors. 20. Surface Modification and Stability of Strong Luminescing CdS Particles. *J. Am. Chem. Soc.* **1987**, *109*, 5649–5655.
- (13) Pong, B.-K.; Trout, B. L.; Lee, J.-Y. Modified Ligand-Exchange for Efficient Solubilization of CdSe/ZnS Quantum Dots in Water: A Procedure Guided by Computational Studies. *Langmuir* **2008**, *24*, 5270–5276.
- (14) Rogach, A. L.; Kornowski, A.; Gao, M.; Eychmüller, A.; Weller, H. Synthesis and Characterization of a Size Series of Extremely Small Thiol-Stabilized CdSe Nanocrystals. *J. Phys. Chem. B* **1999**, *103*, 3065–3069.
- (15) Kapitonov, A. M.; Stupak, A. P.; Gaponenko, S. V.; Petrov, E. P.; Rogach, A. L.; Eychmüller, A. Luminescence Properties of Thiol-Stabilized CdTe Nanocrystals. *J. Phys. Chem. B* **1999**, *103*, 10109–10113.
- (16) Qian, H.; Li, L.; Ren, J. One-step and Rapid Synthesis of High Quality Alloyed Quantum Dots (CdSe–CdS) in Aqueous Phase by Microwave Irradiation with Controllable Temperature. *Mater. Res. Bull.* **2005**, *40*, 1726–1736.
- (17) Qian, H.; Qiu, X.; Li, L.; Ren, J. Microwave-Assisted Aqueous Synthesis: A Rapid Approach to Prepare Highly Luminescent ZnSe(S) Alloyed Quantum Dots. *J. Phys. Chem. B* **2006**, *110*, 9034–9040.
- (18) Schumacher, W.; Nagy, A.; Waldman, W. J.; Dutta, P. K. Direct Synthesis of Aqueous CdSe/ZnS-Based Quantum Dots Using Microwave Irradiation. *J. Phys. Chem. C* **2009**, *113*, 12132–12139.
- (19) Han, H.; Francesco, G. D.; Maye, M. M. Size Control and Photophysical Properties of Quantum Dots Prepared via a Novel Tunable Hydrothermal Route. *J. Phys. Chem. C* **2010**, *114*, 19270–19277.
- (20) Gerbec, J. A.; Magana, D.; Washington, A.; Strouse, G. F. Microwave-Enhanced Reaction Rates for Nanoparticle Synthesis. *J. Am. Chem. Soc.* **2005**, *127*, 15791–15800.
- (21) Roy, M. D.; Herzing, A. A.; DePaoli Lacerda, S. H.; Becker, M. L. Emission-Tunable Microwave Synthesis of Highly Luminescent Water Soluble CdSe/ZnS Quantum Dots. *Chem. Commun.* **2008**, 2106–2108.
- (22) Varshni, Y. P. Temperature Dependence of the Energy Gap in Semiconductors. *Physica* **1967**, *34*, 149–154.
- (23) Kawata, G.; Ogawa, Y.; Minami, F. Density Dependence of Photoluminescence Lifetime of CdSe/ZnS Core–Shell Colloidal Quantum Dots. *J. Appl. Phys.* **2011**, *110*, 064323-1–064323-4.
- (24) Gong, H.-M.; Zhou, Z.-K.; Song, H.; Hao, Z.-H.; Han, J.-B.; Zhai, Y.-Y.; Xiao, S.; Wang, Q.-Q. The Influence of Surface Trapping and Dark States on the Fluorescence Emission Efficiency and Lifetime of CdSe and CdSe/ZnS Quantum Dots. *J. Fluoresc.* **2007**, *17*, 715–720.
- (25) Baranov, A. V.; Rakovich, Y. P.; Donegan, J. F.; Perova, T. S.; Moore, R. A.; Talapin, D. V.; Rogach, A. L.; Masumoto, Y.; Nabiev, I. Effect of ZnS Shell Thickness on the Phonon Spectra in CdSe Quantum Dots. *Phys. Rev. B* **2003**, *68*, 165306.
- (26) Peterson, M. D.; Mooseker, M. S. Characterization of the Enterocyte-like Brush Border Cytoskeleton of the C2BBe Clones of the Human Intestinal Cell Line, Caco-2. *J. Cell. Sci.* **1992**, *102* (Pt 3), 581–600.
- (27) McCracken, C.; Zane, A.; Knight, D. A.; Dutta, P. K.; Waldman, W. J. Minimal Intestinal Epithelial Cell Toxicity in Response to Short- and Long-Term Food-Relevant Inorganic Nanoparticle Exposure. *Chem. Res. Toxicol.* **2013**, *26*, 1514–1525.

- (28) Leadbeater, N. E. In Situ Reaction Monitoring of Microwave-Mediated Reactions Using IR Spectroscopy. *Chem. Commun.* **2010**, *46*, 6693–6695.
- (29) Gaponik, N.; Talapin, D. V.; Rogach, A. L.; Hoppe, K.; Shevchenko, E. V.; Kornowski, A.; Eychmüller, A.; Weller, H. Thiol-Capping of CdTe Nanocrystals: An Alternative to Organometallic Synthetic Routes. *J. Phys. Chem. B* **2002**, *106*, 7177–7185.
- (30) Ziegler, J.; Merkulov, A.; Grabolle, M.; Resch-Genger, U.; Nann, T. High-Quality ZnS Shells for CdSe Nanoparticles: Rapid Microwave Synthesis. *Langmuir* **2007**, *23*, 7751–7759.
- (31) Jiang, F.; Muscat, A. J. Ligand-Controlled Growth of ZnSe Quantum Dots in Water during Ostwald Ripening. *Langmuir* **2012**, *28*, 12931–12940.
- (32) Wang, Y.; Tang, Z.; Correa-Duarte, M. A.; Pastoriza-Santos, I.; Giersig, M.; Kotov, N. A.; Liz-Marzán, L. M. Mechanism of Strong Luminescence Photoactivation of Citrate-Stabilized Water-Soluble Nanoparticles with CdSe Cores. *J. Phys. Chem. B* **2004**, *108*, 15461–15469.
- (33) Jones, M.; Nedeljkovic, J.; Ellingson, R. J.; Nozik, A. J.; Rumbles, G. Photoenhancement of Luminescence in Colloidal CdSe Quantum Dot Solutions. *J. Phys. Chem. B* **2003**, *107*, 11346–11352.
- (34) Torimoto, T.; Nishiyama, H.; Sakata, T.; Mori, H.; Yoneyama, H. Characteristic Features of Size-Selective Photoetching of CdS Nanoparticles as a Means of Preparation of Monodisperse Particles. *J. Electrochem. Soc.* **1998**, *145*, 1964–1968.
- (35) Bakalova, R.; Zhelev, Z.; Jose, R.; Nagase, T.; Ohba, H.; Ishikawa, M.; Baba, Y. Role of Free Cadmium and Selenium Ions in the Potential Mechanism for the Enhancement of Photoluminescence of CdSe Quantum Dots under Ultraviolet Irradiation. *J. Nanosci. Nanotechnol.* **2005**, *5*, 887–894.
- (36) Wang, L.-L.; Jiang, J.-S. Optical Performance Evolutions of Reductive Glutathione Coated CdSe Quantum Dots in Different Environments. *J. Nanopart. Res.* **2011**, *13*, 1301–1309.
- (37) Luan, W.; Yang, H.; Wan, Z.; Yuan, B.; Yu, X.; Tu, S. Mercaptopropionic Acid Capped CdSe/ZnS Quantum Dots as Fluorescence Probe for lead(II). *J. Nanopart. Res.* **2012**, *14*, 1–8.
- (38) Zhang, H.-L.; Li, Y.-Q.; Wang, J.-H.; Li, X.-N.; Lin, S.; Zhao, Y.-D.; Luo, Q.-M. Special Method to Prepare Quantum Dot Probes with Reduced Cytotoxicity and Increased Optical Property. *J. Biomed. Opt.* **2010**, *15*, 015001-1–015001-8.